Aging and sperm signals alter DNA break formation and repair in the *C. elegans* germline

Erik Toraason[1¶], Victoria L. Adler[1¶], and Diana E. Libuda[1,*]

1 University of Oregon, Department of Biology, Institute of Molecular Biology, Eugene, OR, 97403

¶ These authors contributed equally to this work

* Corresponding Author (dlibuda@uoregon.edu)

Short title: DNA break formation and repair in aging oocytes

Abstract

Female reproductive aging is associated with decreased oocyte quality and fertility. The nematode *Caenorhabditis elegans* is a powerful system for understanding the biology of aging and exhibits age-related reproductive defects that are analogous to those observed in many mammals, including dysregulation of DNA repair. *C. elegans* germline function is influenced simultaneously by both reproductive aging and signals triggered by limited supplies of sperm, which are depleted over chronological time. To delineate the causes of DNA repair defects in aged *C. elegans* germlines, we assessed both DNA double strand break (DSB) induction and repair during meiotic prophase progression in aged germlines which were depleted of self-sperm, mated, or never exposed to sperm. We find that germline DSB induction is dramatically reduced only in hermaphrodites which have exhausted their endogenous sperm, suggesting that a signal due specifically to sperm depletion downregulates DSB formation. We also find that DSB repair is delayed in aged germlines regardless of whether hermaphrodites had either a reduction in sperm supply or an inability to endogenously produce sperm. These results demonstrate that in contrast to DSB induction, DSB repair defects are a feature of *C. elegans* reproductive aging independent of sperm presence. Finally, we demonstrate that the ubiquitin E2 ligase variant UEV-2 is required for efficient DSB repair specifically in young germlines, implicating UEV-2 in the regulation of DNA repair during reproductive aging. In summary, our study demonstrates that DNA repair defects are a feature of *C. elegans* reproductive aging and uncovers parallel mechanisms regulating efficient DSB formation in the germline.

Author Summary

Aging leads to a decline in the quality of the female reproductive cells, known as oocytes. Oocytes subjected to reproductive aging experience an increase in both infertility and aneuploidies that cause miscarriages and birth defects. The nematode *Caenorhabditis elegans* is a classic model system used to determine the mechanisms of aging. Old *C. elegans* oocytes accrue many defects which may contribute to their reduced quality, including dysregulation of DNA repair. *C. elegans* fertility and germline function is also regulated oocyte-independently by sperm-dependent signals. To determine how aging and sperm may independently impact DNA repair in aging *C. elegans* oocytes, we control oocyte aging and sperm presence independently to evaluate their effects on DNA break formation and repair. We find that running out of sperm reduces the levels of DNA breaks which are produced, but the efficiency of DNA repair declines during aging independent of sperm effects. We also identify a protein which specifically promotes DNA repair in the oocytes of young animals, suggesting that this protein may regulate DNA repair in the germline during aging. Taken together, our research defines aging-specific and aging-independent mechanisms which regulate the genome integrity of oocytes.

88 **Introduction**

89 Genome integrity must be preserved during gamete development, as any genetic
90 defects incurred may have detrimental effects on progeny or fertility. Meiosis, the specialized
91 cell division that generates haploid gametes such as eggs and sperm, utilizes specific DNA
92 repair pathways to both ensure accurate chromosome segregation and preserve genomic
93 integrity. During early meiotic prophase I, DNA double-strand breaks (DSBs) are intentionally
94 induced across the genome by the conserved topoisomerase-like protein Spo11 (Keeney *et al.*
95 1997; Dernburg *et al.* 1998). A specific subset of these breaks must be repaired by
96 recombination as crossovers, creating the physical connections between homologous
97 chromosomes required for accurate chromosome segregation. Failure to repair meiotic DSBs
98 accurately and efficiently can contribute to infertility or risk the formation of *de novo* germline
99 mutations.

100 Gamete quality is negatively impacted in organisms of advanced chronological age
101 (Broekmans *et al.* 2007). In many organisms, oocyte quality in particular declines starkly with
102 maternal age (Luo *et al.* 2009, 2010; Moghadam *et al.* 2022). Oocyte aging is associated with
103 conserved phenotypic changes, including loss of sister chromatid cohesion, dysregulation of
104 DNA repair gene expression, and derepression of heterochromatin and retroviral elements (Luo
105 *et al.* 2010; Achache *et al.* 2021; Raices *et al.* 2021; Chatzidaki *et al.* 2021; Wasserzug-Pash *et*
106 *al.* 2022).

107 The nematode *Caenorhabditis elegans* is a key model system for the study of aging
108 biology, including age-related infertility (Mack *et al.* 2018). *C. elegans* hermaphrodites (which
109 produce oocytes as adults) undergo reproductive senescence due to declining oocyte quality
110 and incur many of the defects observed in the aging mammalian ovary (Andux and Ellis 2008;
111 Luo *et al.* 2009, 2010; Achache *et al.* 2021). Unlike many mammalian systems, however, which
112 generate oocytes *in utero* and hold them in dictyate arrest until ovulation, *C. elegans*

113 hermaphrodites continuously produce new oocytes during their adult reproductive period (Albert
114 Hubbard and Greenstein 2000). Mitotic proliferation and ovulation of oocytes is dependent upon
115 signals from sperm, which are stored at the end of the germline in a specialized compartment
116 called the 'spermatheca' (Mccarter *et al.* 1999; Cinquin *et al.* 2016). "Obligate female" mutants,
117 which do not produce sperm, therefore exhibit dramatically slowed germline proliferation and
118 progression (Doniach and Hodgkin 1984; Schedl and Kimble 1988; Mccarter *et al.* 1999;
119 Cinquin *et al.* 2016). The *C. elegans* germline is organized in a spatial temporal gradient
120 wherein oocytes mitotically proliferate at the distal tip and move proximally through the germline
121 as they progress through meiotic prophase I (Albert Hubbard and Greenstein 2000).Thus,
122 oocyte nuclei at all stages of meiotic prophase I are simultaneously present in the adult germline
123 and enable assessment of meiotic events which are dynamic across prophase, such as the
124 induction and repair of DSBs.

125 Multiple lines of evidence suggest that preservation of genome integrity is important for
126 the maintenance of oocyte quality during reproductive aging. Human females carrying DNA
127 repair protein variants exhibit extended fertility (Ruth *et al.* 2021). *C. elegans* mutants with
128 extended reproductive periods are also resilient to exogenous DNA damage and upregulate
129 genes associated with DNA repair (Luo *et al.* 2010). Further, recent evidence demonstrated that
130 DNA damage and repair are altered in aged *C. elegans* germlines (Achache *et al.* 2021; Raices
131 *et al.* 2021). By the fourth day of adulthood, *C. elegans* oocyte nuclei exhibit fewer programmed
132 DSBs, delayed loading of recombination proteins, and increased engagement of error-prone
133 repair mechanisms (Achache *et al.* 2021; Raices *et al.* 2021).

134 Sperm also regulate *C. elegans* germline physiology and reproduction. *C. elegans*
135 hermaphrodites produce sperm only during a late stage in larval development (L'Hernault 2006).
136 By the third to fourth day of adulthood, these sperm are depleted, which leads to a premature
137 cessation of reproduction in *C. elegans* hermaphrodites (Luo *et al.* 2010). Sperm depletion also

138 induces broad transcriptional remodeling independent of aging processes, resulting in a 'female-
139 like' transcriptional profile (Angeles-Albores *et al.* 2017). Mating extends the hermaphrodite
140 reproductive span on average to the sixth day of adulthood, after which declining oocyte quality
141 limits fertility (Luo *et al.* 2010). Mating and even exposure to males, however, also induces
142 deleterious responses in hermaphrodites leading to premature demise (Maures *et al.* 2014; Shi
143 and Murphy 2014). It remains unknown how reproductive aging, signaling induced by the
144 presence or depletion of sperm, and mating intersect to regulate meiotic processes in aged *C.*
145 *elegans* germlines.

146 To define DNA repair defects which are specific to reproductive aging, we assayed
147 levels of DSB formation and repair in the meiotic oocytes of aged mated and unmated *C.*
148 *elegans* hermaphrodites, as well as feminized germline mutants that do not produce sperm (*fog-*
149 *2* mutants). We demonstrate that while the depletion of sperm downregulates DSB induction in
150 aged germlines, delayed DSB repair is a shared feature of aging germlines independent of
151 sperm presence. Finally, we identify the ubiquitin E2 ligase variant protein UEV-2 as a putative
152 regulator of DNA repair during germline aging. Taken together, our work distinguishes DNA
153 repair defects specific to reproductive aging and identifies parallel mechanisms regulating
154 gamete quality in the immortal germline.

155

156 **Methods**

157 ***Caenorhabditis elegans* strains and maintenance**

158 *Caenorhabditis elegans* strains were maintained at 20°C on nematode growth medium (NGM)
159 plates seeded with OP50 *Escherichia coli* bacteria. All experiments were performed in the N2
160 genetic background. Strains used in this experiment include AV761 (*GFP::cosa-1* II; *spo-*
161 *11(me44)* IV/ nT1[qIs51]), AV676 (*GFP::cosa-1* II; *fog-2(q71)* V), N2 (wildtype), CB4108 (*fog-*

162 *2(q71)* V*)*, DLW135 (*uev-2(gk960600gk429008gk429009); rgr-1(gk429013)* III), DLW199
163 (liblS4[*pie-1p::uev-2::unc-54 3'UTR*] III:7007600), N2 (wild type), VC30168 (Million Mutation
164 Project strain carrying *uev-2(gk960600)*), and WBM1119 (wbmIs60 [*pie-1p::3XFLAG::dpy-10*
165 *crRNA::unc-54* 3'UTR] (III:7007600)).

166 In experiments with aged animals, L4 hermaphrodites were isolated and maintained on NGM
167 plates seeded with OP50 in the absence of males. Strains which produced self progeny were
168 transferred to new NGM plates seeded with OP50 2 days post-L4 to prevent overconsumption
169 of food from F1 progeny. At this transfer, if the experimental cohort was to be mated, young
170 adult male N2 worms were additionally added to these plates at a ratio of ~1.5-2 males per
171 hermaphrodite. Mated hermaphrodites were again transferred to new NGM plates with OP50
172 ~20-26 hours after males were added and male animals were discarded.

173 Strain DLW135 was generated by backcrossing VC30168 to N2 10 times. VC30168 was
174 created by the Million Mutations Project (Thompson *et al.* 2013) and carried many mutations in
175 addition to the *uev-2(gk960600)* allele of interest. Following backcrossing, mutations on
176 Chromosomes I, II, IV, V, and X were assumed to have been eliminated. To determine the
177 success of backcrossing on removing undesired mutations *in cis* with *uev-2* on Chromosome III,
178 we assessed the presence of known flanking mutations to *uev-2(gk960600gk429008gk429009)*.
179 Presence of the upstream most proximal genic mutation to *uev-2*, *pho-9(gk429005)*, was
180 assessed via PCR amplification using OneTaq 2x Master Mix (forward primer DLO1142 5'-
181 ACCCATTTCCCATTCAATCA-3' reverse primer DLO1143 5'-TTGTAATCTGCCCCAAAAGG-3')
182 and subsequent HpaII restriction digest (New England Biolabs). DLW135 carried a wild type
183 allele of *pho-9*, indicating that the region of Chromosome III upstream of *uev-2* was successfully
184 reverted to wild-type sequence by recombination. However, the closely linked (~1 cM)
185 downstream allele *rgr-1(gk429013)* was preserved in DLW135, as confirmed by Sanger
186 sequencing (Sequetech) of a PCR amplified region of the *rgr-1* locus using OneTaq 2x Master

187 Mix (forward primer DLO1140 5'-TGGAATGGGACTTCCTCTTG-3' reverse primer DLO1141 5'-
188 TTTCCAAAAGCCAGGACATC-3') isolated using a GeneJET PCR Purification kit
189 (ThermoFisher). The *rgr-1(gk429013)* allele is a single base pair substitution resulting in a
190 S360N missense mutation. RGR-1 is a Mediator complex subunit involved in transcriptional
191 activation that is required for embryonic viability (Shim *et al.* 2002). S360N does not disrupt a
192 predicted functional domain, and mutants carrying *rgr-1(gk429013)* survive embryogenesis and
193 are fertile, indicating that this mutation does not severely disrupt function of the RGR-1 protein.
194 As RGR-1 is not known to play a role in DNA damage repair, and *uev-2* has been previously
195 demonstrated to modulate germline sensitivity to DNA damage (Luo *et al.* 2010), the
196 phenotypes we observed using DLW135 in this manuscript are not best explained by the
197 presence of the *rgr-1(gk429103)* mutation. For simplicity, DLW135 mutants are referred to as
198 '*uev-2* mutants' in the text of this manuscript.

199 **CRISPR/Cas9 genome editing**

200 Strain DLW199 was generated using the SKILODGE transgenic system (Silva-García *et al.*
201 2019). WBM1119 was injected with 40ng/μL pRF4 purified plasmid, 40ng/μL purified PCR
202 amplicon of the full *uev-2* coding sequence with 35bp homology arms to the wbmIs60 landing
203 site (Phusion polymerase, forward primer DLO1144 5'-
204 tcccaaacaattaaaaatcaaattttcttttccagATGCGAAGACGTAGCAACAG-3' reverse primer DLO1154
205 5'-taattggacttagaagtcagaggcacgggcgcgagatgTTAGTTTTCGATGTCAATTGGT-3'), 0.25 μg/μL
206 Cas9 enzyme (IDT), 100ng/μL tracrRNA (IDT), and 56ng/μL crRNA DLR002 (5'-
207 GCUACCAUAGGCACCACGAG-3'). Dpy F1 progeny were isolated and screened for insertion
208 at the wbmIs60 locus by PCR following the SKILODGE recommended protocols (primers
209 CGSG130, CGSG117 (Silva-García *et al.* 2019)).

210 The candidate insertion identified among progeny from the above injected hermaphrodites
211 contained an undesired additional 43bp of sequence between the 5' 3xFLAG tag of the edited

212 wbmIs60 landing site and the start codon of the *uev-2* coding sequence. The strain carrying this
213 insertion allele was backcrossed 3x to N2 and was CRISPR/Cas9 edited again to remove the
214 undesired 5' sequence. Worms were injected with 0.25 μg/μL Cas9 (IDT), 100ng/μL tracrRNA
215 (IDT), 28ng/μL gRNA DLR022 (5'-GAUCUUUAUAAUCACCGUCA-3'), 28ng/μL gRNA DLR023
216 (5'-UGUUGCUACGUCUUCGCAUC-3'), 25ng/μL ssODN donor DLO1173 (5'-
217 AACAATTAAAAATCAAATTTTCTTTTCCAGATGCGGAGGCGAAGTAATAGACAATATGTTGA
218 TCTCTCATATTTTCGCGAAAC-3'), and 40ng/μL purified pRF4 plasmid. Successful removal of
219 the 3xFLAG sequence and undesired 43bp inserted sequence were confirmed by PCR and
220 Sanger sequencing (Sequetech).

221 **Nematode irradiation**

222 *C. elegans* worms were maintained at 20°C on NGM plates seeded with OP50 prior to and
223 following irradiation. Irradiation was performed using a Cs^{137} source (University of Oregon).

224 **Immunofluorescence sample preparation and microscopy**

225 Immunofluorescence samples were prepared as in (Libuda *et al.* 2013). Nematodes were
226 dissected in 1x Egg Buffer (118 mM NaCl, 48 mM KCl_2, 2 mM $CaCl_2$, 2 mM $MgCl_2$, 25 mM
227 HEPES pH7.4, 0.1% Tween20) and were fixed in 1x Egg Buffer with 1% paraformaldehyde for 5
228 min on a SuperFrost Plus slide (VWR). Slides were then flash frozen in liquid nitrogen and the
229 cover slip was removed before the slides were placed in ice cold methanol for 1 minute. Slides
230 were washed in 1xPBST (1x PBS, 0.1% Tween20) 3x for 10 minutes before they were placed in
231 Block (1xPBST with 0.7% bovine serum albumin) for a minimum of one hour. 50μL of primary
232 antibody diluted in PBST (see below for specific antibody dilutions) was then placed on each
233 slide and samples were incubated for 16-18hrs in a dark humidifying chamber with parafilm
234 coverslips. Slides were then washed 3x in 1xPBST for 10 minutes. 50μL of secondary antibody
235 diluted 1:200 in PBST were then added to each sample and slides were incubated for 2hr in a

236 dark humidifying chamber with parafilm coverslips. Slides were washed 3x in 1xPBST for 10
237 minutes, and then 50μL of 2μg/mL DAPI was applied to each slide. Samples were incubated in
238 a dark humidifying chamber with parafilm coverslips for 5 minutes, then were washed 1x in
239 PBST for 5 minutes. Slides were mounted with a No 1.5 coverslip (VWR) and sealed with nail
240 polish. All slides were maintained at 4°C until imaging.

241 Immunofluorescence images were acquired at 512x512 or 1024x1024 pixel dimensions on an
242 Applied Precision DeltaVision microscope with a 63x lens and a 1.5x optivar. All images were
243 acquired in 3 dimensions with Z-stacks at 0.2μm intervals. In a minority of aged unirradiated
244 germlines, we noted that most nuclei in mid-late pachytene exhibited high levels of RAD-51 and
245 condensed DNA morphology characteristic of apoptosis. These aberrant gonads were not
246 included in our analyses. Images were deconvolved with Applied Precision softWoRx software
247 and individual image tiles were stitched into a single image for analysis using the Grid/Collection
248 Stitching module in Fiji with regression threshold 0.7 (Preibisch *et al.* 2009) or using Imaris
249 Stitcher software (Bitplane).

250 Specific antibodies used and their dilution factors are: Rabbit αRAD-51 (1:500), Chicken αRAD-
251 51 (1:1000), Rabbit αDSB-2 (1:5000) (Rosu *et al.* 2013), Rabbit αGFP (1:1500), Chicken
252 αGFP(1:1000), Alexa Fluor 488 Goat αChicken (1:200), Alexa Fluor 555 Goat αChicken (1:200),
253 Alexa Fluor 555 Goat αRabbit (1:200), and Alexa Fluor 488 Goat αRabbit (1:200).

254 **Image analysis and quantification**

255 Images were analyzed as described in (Toraason *et al.* 2021). Image quantification was
256 performed using Imaris software (Bitplane). Individual nuclei within stitched gonads were
257 identified as Surface objects (Smooth 0.1-0.15, Background 3-4, Seed Point Diameter 3-4)
258 based on DAPI staining intensity. Manual thresholding of specific values were used per gonad
259 to generate surfaces which represented the nuclei observed. Defined surfaces were then split to

260 designate individual nuclei using the Imaris Surfaces Split module. Nuclei which were partially
261 imaged or overlapped with other nuclei were eliminated from the analysis. RAD-51 foci were
262 defined as Spot objects (Estimated XY Diameter 0.1, Model PSF-elongation 1.37, Background
263 Subtraction enabled). To determine the number of RAD-51 foci per nucleus, we either utilized
264 the "Find Spots Close to Surface" MATLAB module (Threshold value 0.1) or utilized the "Closest
265 Distance to Surface" statistic calculated by Imaris to find the number of Spots ≤0.1μm distant
266 from nuclei. The length of each germline was defined using the Imaris Measurements tool.
267 Measurement points were specifically placed at the beginning of the premeiotic tip and the end
268 of pachytene. For germlines which had a defined transition zone by DAPI morphology, points
269 were also placed at the start and end of the transition zone.

270 Nuclei positions were transformed from 3D coordinates to a linear order using the Gonad
271 Linearization Algorithm implemented in R (Toraason *et al.* 2021). Gonad length in germlines
272 which lacked a defined transition zone (e.g. *fog-2* mutants, Supplemental Figure 2) was
273 normalized to the distance from the premeiotic tip to the end of pachytene, where the premeiotic
274 tip begins at position 0 and the end of pachytene is at position 1. In all other germlines, the
275 gonad length was normalized to pachytene, where the beginning of pachytene is position 0 and
276 the end of pachytene is position 1.

277 Germline DSB-2 staining was analyzed in Imaris using germlines stitched in Fiji as described
278 above. The length of the germline was defined using the Imaris Measurements tool. Specific
279 points were placed at the beginning of the transition zone, end of the transition zone, beginning
280 of the DSB-2 zone (defined as the row of nuclei in which most nuclei had DSB-2 staining), the
281 end of the DSB-2 zone, the final position of one or more nuclei which had DSB-2 staining, and
282 the end of pachytene. The measured distances were then normalized to pachytene, where the
283 beginning of pachytene is position 0 and the end of pachytene is position 1.

284 GFP::COSA-1 foci were quantified manually from late pachytene nuclei from 3D z-stacks using
285 Fiji. Nuclei that were completely contained within the image stack were quantified in the last few
286 rows of the late pachytene region in which all nuclei displayed bright GFP::COSA-1 foci (last ~3-
287 6 rows of late pachytene in old *fog-2* germlines, last ~6-8 rows of late pachytene in young *fog-2*
288 germlines).

289 ***fog-2* Brood Viability Assay**

290 *C. elegans* worms were maintained at 20°C during fertility assays. Feminized *fog-2* mutants
291 were synchronized in age by placing gravid mated CB4108 females onto an NGM plate seeded
292 with OP50 for one hour. Hatched female progeny were isolated as L4s from these plates and
293 were kept in isolation from males to prevent mating. At adult day 1, 2, 3, 4, or 5, these isolated
294 *fog-2* females were then placed on individual plates with n=2 young adult N2 males each. Mated
295 *fog-2* females were then subsequently transferred to new NGM plates seeded with OP50 with
296 young adult N2 males at either 6hr, 12hr, 18hr, 24hr, and 48hr after the first mating, or at 24hr
297 and 48hr after the first mating. 72hr after the first mating, adult females were discarded. Plates
298 were scored ~24hr after the parent female was removed for hatched progeny, dead eggs, and
299 unfertilized oocytes. Brood viability was calculated as (hatched progeny) / (hatched progeny +
300 dead eggs). Fertility assays were replicated twice with n=5 females of each age group assayed
301 per replicate.

302 During the course of the brood viability assays, some mated *fog-2* females exhibited matricidal
303 hatching. This phenotype was more pronounced in aged worms, consistent with previous work
304 which showed that matricidal hatching is exacerbated with maternal age (Pickett and Kornfeld
305 2013). Only eggs which were successfully ovulated were scored in the assay.

306 **Statistics**

307 All statistics were calculated in R (v4.0.3). Data wrangling was performed using the Tidyverse
308 package (v1.3.0) (Wickham *et al.* 2019). Specific statistical tests used are denoted in the figure
309 legends and text. P values were adjusted for multiple comparisons when appropriate. If 3
310 pairwise comparisons were being performed, Bonferroni correction was applied. If >3 pairwise
311 comparisons were performed, Holm-Bonferroni correction was instead applied to reduce the risk
312 of type II statistical errors.

313 **Data and Code Availability**

314 The gonad linearization algorithm is available on the Libuda Lab GitHub
315 <github.com/libudalab/Gonad-Analysis-Pipeline> and on the Libuda Lab website
316 <libudalab.org>

317

318 **Results**

319 **Meiotic DNA break levels are influenced by both aging and sperm depletion**

320 To determine the relative contributions of reproductive aging and sperm depletion to
321 DNA break repair dynamics in the *C. elegans* germline, we examined DNA break levels in the
322 oocytes of aged hermaphrodites which were mated (to prevent sperm depletion) or unmated (to
323 permit sperm depletion) (Figure 1A). DNA breaks were quantified using immunofluorescence to
324 visualize the recombinase RAD-51, which marks DSBs designated for repair by recombination
325 (Gartner and Engebrecht 2022). While the cytological appearance of RAD-51 foci indicates the
326 occurrence of DSBs, disappearance of RAD-51 foci indicates progression of a DSB event
327 further through a DSB repair pathway. “Young” germlines were isolated from N2 hermaphrodites
328 on the first day of adulthood (1 day post-L4, Figure 1A), while “aged” germlines were isolated
329 from N2 hermaphrodites on their fourth day of adulthood (4 days post-L4, Figure 1A). Aged

330 hermaphrodites were maintained either unmated to males, or mated with males from their
331 second to third day post-L4 larval stage (Figure 1A, see Methods).

332 To quantify the profile of DSB induction and repair across prophase I, we counted the
333 number of RAD-51 foci per nucleus in oocytes from young and aged animals throughout the
334 germline (see Methods). Under normal conditions, RAD-51 foci accumulate within nuclei
335 following DSB induction by the conserved endonuclease SPO-11 in early pachytene (Dernburg
336 *et al.* 1998; Colaiácovo *et al.* 2003). Then, as nuclei progress through mid and late pachytene,
337 these RAD-51 foci decline in number as DSBs are repaired (Colaiácovo *et al.* 2003). During
338 early pachytene, the amount of RAD-51 foci per nucleus was similar between aged mated
339 germlines and young germlines (Figure 1B-C, Bin 2 Mann-Whitney U test $p=0.258$). Young
340 germlines, however, accumulated a higher total number of RAD-51 foci per nucleus (Figure 1B-
341 C, Bin 3 Mann-Whitney U test $p=0.005$), suggesting that DSB induction or RAD-51 loading is
342 slightly compromised in aged mated germlines. We further noted that RAD-51 foci in aged
343 unmated germlines were greatly decreased throughout early pachytene as compared to both
344 young and aged mated germlines (Figure 1B-C, Bins 2-3 Mann-Whitney U test $p<0.001$),
345 indicating that sperm depletion in aged germlines may affect meiotic DSB induction and/or RAD-
346 51 loading.

347 In contrast to early pachytene, nuclei throughout mid pachytene from aged mated
348 germlines maintained higher levels of RAD-51 than young germlines (Figure 1B-C, Bins 4-5
349 Mann-Whitney U test $p<0.05$). We observed a similar effect in the aged unmated germlines,
350 which also displayed elevated numbers of RAD-51 foci relative to young germlines throughout
351 mid pachytene (Figure 1B-C, Bins 4-5 Mann-Whitney U test $p<0.001$). Thus, DSB repair at mid-
352 pachytene may be delayed in aging germlines regardless of mating or sperm depletion. Notably,
353 by late pachytene the number of RAD-51 foci per nucleus converged between young, aged
354 mated, and aged unmated germlines (Figure 1B-C, Bin 6 Mann-Whitney U test $p>0.05$),

355 indicating that ultimately all DSBs can be repaired or minimally offload RAD-51 in aged
356 germlines. Taken together, our results suggest that parallel mechanisms may regulate DNA
357 break levels in aged *C. elegans* germlines: 1) depletion of sperm downregulates DSB induction
358 and/or RAD-51 loading; and, 2) reproductive aging delays RAD-51 foci unloading at mid
359 pachytene.

360 To determine if the persistent RAD-51 foci in aged mated and unmated germlines were
361 derived from the programmed meiotic DSBs, we also examined RAD-51 foci in *spo-11(me44)*
362 null mutants, which do not form meiotic DSBs (Supplemental Figure 1) (Colaiácovo *et al.* 2003).
363 We did not observe a notable increase in nuclei with RAD-51 foci in aged *spo-11* germlines,
364 indicating that the persistent RAD-51 foci present at mid pachytene in aged wildtype gonads are
365 likely derived from normal meiotic functions and processes, such as SPO-11 activity.

366 Nuclei which are competent for DSB induction in the *C. elegans* germline have their
367 chromatin marked with the protein DSB-2 (Rosu *et al.* 2013). To assess if the altered
368 accumulation of DSBs which we observed in aged unmated germlines coincided with a change
369 in competency for DSB induction, we quantified the extent of young and aged germlines in
370 which ≥50% of nuclei exhibited DSB-2 staining (the "DSB-2 zone", Supplemental Figure 2A-B).
371 DSB-2 accumulates on meiotic chromatin beginning in the transition zone (leptotene/zygotene)
372 and is offloaded from the majority of nuclei by mid pachytene (Rosu *et al.* 2013; Toraason *et al.*
373 2021). Mutants which incur errors in crossover formation, however, maintain DSB-2 on meiotic
374 chromatin later into pachytene (Rosu *et al.* 2013). While the length of the DSB-2 zone was only
375 subtly altered in aged mated germlines (Supplemental Figure 2B-C, Mann-Whitney U test
376 $p=0.027$), the DSB-2 zone persisted later into pachytene in aged unmated germlines relative to
377 young germlines (Supplemental Figure 2B-C, Mann-Whitney U test $p=0.008$). Thus, our data
378 indicate that the extent of DSB-2 marked pachytene nuclei is influenced both by aging and by
379 the absence of sperm.

380 **Meiotic DNA breaks are elevated in aged feminized germlines**

381 To uncouple the relationship between sperm depletion and reproductive aging in
382 regulating DSB induction and repair, we examined RAD-51 levels in germlines which have
383 never been impacted by sperm or mating. Hermaphrodites carrying the *fog-2(q71)* mutation do
384 not produce sperm during larval development but proliferate a full adult complement of oocytes
385 (Schedl and Kimble 1988), rendering them "obligate females." Due to the absence of signaling
386 from sperm in *fog-2* mutants, both germline stem cell proliferation and meiotic progression are
387 halted, such that meiotic oocytes are held within the gonad (Mccarter *et al.* 1999; Cinquin *et al.*
388 2016). Nonetheless, feminized mutants undergo reproductive senescence and exhibit reduced
389 oocyte quality with age (Supplemental Figure 3; (Andux and Ellis 2008; Luo *et al.* 2009))

390 We analyzed the levels of RAD-51 foci in oocyte nuclei from young (1 day post-L4),
391 aged (4 days post-L4), and old (6 days post-L4) *fog-2* germlines (Figure 2A-B). During our
392 experiments we noted that the cytologically distinctive transition zone, which demarcates
393 meiotic entry and is composed of nuclei undergoing active chromosome movement to facilitate
394 pairing, was dramatically reduced in aged *fog-2* germlines (Supplemental Figure 4). Previous
395 work has shown that mitotic germ cell proliferation is reduced in feminized and sperm-depleted
396 germlines (Cinquin *et al.* 2016). Thus, the absence of a transition zone in aged *fog-2* germlines
397 may be the product of two parallel effects: 1) nuclei in the transition zone completing the pairing
398 process and therefore exhibiting the classic "cage-like" morphology of paired chromosomes
399 found in pachytene nuclei; and, 2) decreased proliferation also limiting the number of new nuclei
400 which enter meiosis. This lack of the transition zone in aged *fog-2* germlines presented a
401 challenge for staging meiotic nuclei to make comparisons between young and aged gonads. To
402 quantify RAD-51 levels in *fog-2* germlines independent of meiotic stages, we normalized the
403 germline length with position 0 at the premeiotic tip and position 1 at the end of pachytene and
404 used a sliding window to assay RAD-51 foci within the germline (Figure 2D, see Methods)

405 (Toraason *et al.* 2021). To describe the RAD-51 profile of aging *fog-2* germlines, we calculated
406 two metrics: 1) the "RAD-51 zone" indicating the extent of the germline which contained nuclei
407 with RAD-51 foci; and, 2) the "peak RAD-51 window" indicating the maximum levels of RAD-51
408 within the germlines.

409 To assess whether the proportion of germline nuclei with RAD-51 foci was altered in
410 aging *fog-2* germlines, we calculated the "RAD-51 zone" of each age group, which was defined
411 as the germline distance extending from the most distal (near the premeiotic tip) to the most
412 proximal (near the end of pachytene) windows in which at least 50% of nuclei had one or more
413 RAD-51 foci (Figure 2B, 2D). We found that the RAD-51 zone extended more distally in the
414 germline in aged and old *fog-2* animals as compared to young germlines (Figure 2B, 2D). This
415 distal expansion of the RAD-51 zone can likely be explained by transition zone nuclei in young
416 germlines completing the pairing process and entering pachytene as the germline ages. In
417 contrast, the proximal end of the RAD-51 zone only subtly shifted distally in aged and old
418 germlines (Figure 2B, 2D). This result indicates that later prophase I nuclei within aged *fog-2*
419 germlines continue to either maintain or induce RAD-51 marked DSBs.

420 To determine if the number of RAD-51 marked DSBs in *fog-2* germline nuclei were
421 altered with age, we identified the "peak RAD-51 windows" in each age group, defined as the
422 window in which the mean RAD-51 foci per nucleus was highest (Figure 2C, 2D arrowheads).
423 We noted that the position of the peak RAD-51 window moved distally in aged and old *fog-2*
424 germlines (Figure 2D arrowheads), suggesting that the spatial regulation of DSB induction and
425 repair may change as feminized germlines age. The number of RAD-51 foci per nucleus within
426 the peak RAD-51 window was not significantly different in aged germlines as compared to
427 young gonads (Figure 2C-D, Mann-Whitney U test p=1.000). Old germlines, however, exhibited
428 a significant ~1.5 fold increase in RAD-51 foci per nucleus as compared to young and aged
429 germlines within the peak RAD-51 window, indicating that *fog-2* mutant germ cells accumulate

430 RAD-51 foci during aging (Figure 2C-D, Mann-Whitney U test p <0.001). This result notably
431 differs from aged unmated wildtype germlines, which exhibit reduced DSBs with age (Figure 1B-
432 C) (Achache *et al.* 2021; Raices *et al.* 2021). Our data therefore support a model in which sperm
433 depletion, rather than absence of sperm, downregulates meiotic DSB induction.

434 **DSB repair is altered in aged feminized germlines**

435 The accumulation of RAD-51 foci observed in aging *fog-2* germlines may be the product
436 of: 1) increased induction of DSBs; 2) defects in DSB repair; or, 3) a combination of these
437 effects. To assess the efficiency of DSB repair during *fog-2* germline aging, we exposed young
438 (1 day post-L4) and aged (4 days post-L4) *fog-2* mutant females to 5000 Rads of ionizing
439 radiation (Figure 3A, Supplemental Figure 5), inducing ~118 DSBs per nucleus throughout the
440 germline (Yokoo *et al.* 2012). We then allowed the animals to age for 2 days to resolve this DNA
441 damage before assessing germlines for persistent unrepaired DSBs as marked by RAD-51 foci
442 (Figure 3A). As *fog-2* germlines accumulate DSBs during aging (Figure 2C-D), we established
443 baseline levels of DNA damage based on comparing RAD-51 foci in animals of equivalent ages
444 that were never exposed to radiation to the irradiated cohorts (Figure 3A). We noted
445 considerable inter-nucleus variance in the RAD-51 foci, which persisted following irradiation in
446 both young and aged germlines (Supplemental Figure 5). This effect was particularly prominent
447 in the distal germlines of both groups (Supplemental Figure 5C-D), suggesting that a
448 subpopulation of nuclei in the mitotic germline or early stages of meiosis are uniquely
449 susceptible to exogenous DNA damage regardless of parental age.

450 To estimate the residual DSBs derived from irradiation which were not yet repaired two
451 days post irradiation, we calculated the median number of RAD-51 foci in a sliding window
452 across the germline (Figure 3B, see Methods) and subtracted the unirradiated median RAD-51
453 foci from the irradiated median RAD-51 foci in each window (Figure 3C). Both young and aged
454 germlines maintain high levels of damage in the distal germline following irradiation (germline

455 position 0.0-0.5, Figure 3C, Supplemental Figure 5C). Nuclei in the proximal region of young
456 irradiated germlines did not consistently maintain median DNA break levels higher than
457 baseline; whereas aged irradiated germlines maintained a median elevation of ~6-10 RAD-51
458 foci per nucleus (germline position 0.5-1.0, Figure 3C). This result indicates that aged *fog-2*
459 germlines exhibit DNA repair defects specifically in nuclei at later stages of meiotic prophase I.
460 Taken together, our experiments in "feminized" germlines demonstrate that DNA repair
461 efficiency is altered in aging germlines independent of any signals from sperm.

462 Defects in meiotic DSB repair may disrupt the formation of interhomolog crossovers
463 (Gartner and Engebrecht 2022). To determine if crossover recombination is impeded in aged
464 *fog-2* germlines, we quantified bright GFP::COSA-1 foci, which mark joint molecules designated
465 to become crossovers at late pachytene (Yokoo *et al.* 2012). Under normal conditions, each of
466 the six pairs of *C. elegans* homologous chromosomes form one crossover and therefore most
467 nuclei exhibit only six COSA-1 foci (Yokoo *et al.* 2012). We observed that the number of COSA-
468 1 foci in late pachytene nuclei of old *fog-2* gonads were altered relative to their young
469 counterparts (Figure 4A, Chi square test p=0.033), with a subtle but significant increase
470 specifically in the fraction of nuclei with 7 COSA-1 foci (Figure 4A, Fisher's Exact test p=0.038).
471 Thus, our data suggests that DSB repair in old *fog-2* germlines may be altered in a manner
472 which impacts the number of designated crossovers. Further, the late pachytene region of the
473 germline with bright COSA-1 foci was reduced in old *fog-2* germlines (Figure 4B). This
474 phenotype is reminiscent of synapsis deficient mutants, which form COSA-1 foci only in a very
475 small region of late pachytene (Cahoon *et al.* 2019). Previous work has shown that aged
476 unmated wildtype germlines incur defects in crossover formation which reduce the number of
477 crossovers formed (Luo *et al.* 2010; Achache *et al.* 2021; Raices *et al.* 2021). Our results in *fog-*
478 *2* mutants therefore demonstrate that these defects are not shared in aged feminized *C.*

479 *elegans* germlines, suggesting that sperm presence influences the germ cell capacity for
480 crossover formation during reproductive aging.

481 **UEV-2 is required for 'youthful' germline DSB repair**

482 To identify proteins which may regulate DSB repair in the aging *C. elegans* germline, we
483 looked to candidate genes upregulated in long-reproductive *sma-2* mutant oocytes, which
484 exhibit DNA damage resilience in addition to delayed reproductive senescence (Luo *et al.*
485 2010). The *sma-2* DNA damage resilience phenotype requires upregulation of the ubiquitin E2
486 ligase variant UEV-2, suggesting that this protein may promote efficient germline DNA repair
487 (Luo *et al.* 2010). UEV proteins lack a catalytic cysteine residue conserved in E2 ubiquitin
488 ligases (Sancho *et al.* 1998) but have been shown to form heterodimeric complexes with other
489 E2 ubiquitin ligases to influence their function, implying regulatory roles for this protein class
490 (Vandemark *et al.* 2001; Wijk and Timmers 2010).

491 To assess the influence of UEV-2 on DSB repair during germline aging, we utilized a
492 strain carrying the putative null allele *uev-2(gk960600)*, which ablates the translation initiation
493 site and second exon boundary of the gene (Supplemental Figure 6; see Methods). With the
494 *uev-2* mutant strain, we examined the number of RAD-51 foci in germline nuclei derived from
495 young (1 day post-L4) or aged (4 days post-L4) animals (Figure 5A). Aged *uev-2* mutants were
496 also mated to avoid the DSB induction defects associated with sperm depletion (Figure 5A). If
497 UEV-2 functions to promote efficient DSB repair in young gonads but becomes dysregulated or
498 loses function during aging, then we would expect *uev-2* mutants to exhibit defects in DSB
499 repair in young germlines but minimal additional defects in aged germlines. Indeed, when we
500 compared the levels of RAD-51 observed in young and aged mated wildtype and *uev-2*
501 germlines, we observed DSB repair defects that did not accumulate with age. In early
502 pachytene, young and aged *uev-2* mutants exhibited similar levels of RAD-51 to young wildtype
503 germlines (Figure 5B-C, Bins 2-3 Mann-Whitney U test $p>0.05$), indicating that UEV-2 is not

504 required for meiotic DSB induction nor RAD-51 loading. In contrast, at mid pachytene, young
505 *uev-2* mutant germlines maintained elevated RAD-51 foci relative to young wildtype germlines
506 (Figure 5B-C, Bins 4-5 Mann-Whitney U test $p<0.05$). The specific levels of DSBs at mid
507 pachytene in young *uev-2* mutants were also indistinguishable from aged wildtype germlines
508 (Figure 5B-C, Bins 4-5 Mann-Whitney U test $p>0.05$). These results at mid pachytene indicate
509 that DSB repair is delayed in young *uev-2* mutants to an extent which recapitulates the effect we
510 observe during wildtype aging. Aged *uev-2* germline RAD-51 levels at mid pachytene were
511 statistically indistinguishable from either young or aged mated wildtype germlines (Figure 5B-C,
512 Bins 4-5 Mann-Whitney U test $p>0.05$), suggesting that the *uev-2* mutation does not grossly
513 exacerbate DSB repair defects with age.

514 In late pachytene, the specific rates of DSB resolution diverged slightly between young
515 and aged *uev-2* and wildtype germlines (Figure 5B-C, Bins 6-7 Mann-Whitney U test $p<0.05$),
516 suggesting that UEV-2-independent and age-specific effects may contribute to DSB resolution
517 at this meiotic stage. Taken together, our results indicate that loss of *uev-2* in young germlines
518 is sufficient to phenocopy the mid-pachytene patterns of DSB repair observed in an aged
519 wildtype context. This observation supports a model in which UEV-2 functions in young
520 germlines specifically to promote efficient DSB repair.

521 **Overexpression of *uev-2* alters RAD-51 foci levels in an aged oocytes**

522 As loss of *uev-2* in young germlines appeared to “prematurely age” RAD-51 foci
523 patterns, we hypothesized that overexpression of *uev-2* in aged germlines could ameliorate
524 persistent RAD-51 foci at mid pachytene. To test this hypothesis, we used CRISPR/Cas9
525 genome editing to generate a germline-specific overexpression construct of *uev-2* driven by the
526 *pie-1* promoter (*pie-1p::uev-2*, see Methods). We then assessed for the presence of DSBs as
527 marked by RAD-51 in the germlines of young (1 day post-L4) or aged (4 days post-L4) mated

528 animals overexpressing UEV-2 and compared those levels to young and aged mated wildtype
529 germlines (Figure 6A).
530 At the beginning of early pachytene, both young and aged mated *pie-1p::uev-2* mutants
531 initially accumulated DSBs at levels similar to young and aged mated wildtype gonads (Figure
532 6B-C, Bin 2 Mann-Whitney U test $p>0.05$). However, aged mated *pie-1p::uev-2* mutants
533 accumulated fewer total DSBs than young wildtype, aged mated wildtype, and young *pie-*
534 *1p::uev-2* germlines (Figure 6B-C, Bin 3 Mann-Whitney U test $p<0.05$). At mid pachytene, young
535 *pie-1p::uev-2* germlines maintained elevated RAD-51 foci over young wildtype germlines,
536 suggesting that overexpression of *uev-2* deleteriously impacted DSB repair in this context
537 (Figure 6B-C, Bin 4-5 Mann Whitney U test $p\leq0.001$). This effect was not preserved in aged
538 mated *pie-1p::uev-2* germlines, which exhibited similar DSB levels as young wildtype germlines
539 at the beginning of mid pachytene and slightly elevated foci at the end of mid pachytene (Figure
540 6B-C, Mann-Whitney U test Bin 4 $p=0.156$ Bin 5 $p=0.023$).
541 Throughout late pachytene, young *pie-1p::uev-2* germlines maintained subtle but
542 significantly elevated DSBs relative to young and aged wildtype germlines (Figure 6B-C, Bin 6-7
543 Mann-Whitney U test $p<0.05$). Conversely, aged mated *pie-1p::uev-2* germlines maintained
544 significantly fewer RAD-51 foci throughout late pachytene than young wildtype or young *pie-*
545 *1p::uev-2* germlines (Figure 6B-C, Bin 6-7 Mann-Whitney U test $p<0.05$). Taken together, these
546 data suggest that UEV-2 is not the sole regulator of DSB repair efficiency during *C. elegans*
547 germline aging and appears to have age-dependent functions in regulating meiotic DSB
548 accumulation and repair.
549
550 **Discussion**
551 *C. elegans* germline function is impacted both by reproductive aging and sperm signals.
552 Our study demonstrates that aged *C. elegans* germlines exhibit delayed DSB repair in mid-
553 pachytene regardless of mated status, suggesting that deficiencies in germline DNA repair are a

554 product of reproductive aging. We further find that sperm depletion, but not absence of sperm,
555 reduces RAD-51 marked DSBs at early pachytene, suggesting that loss of signals from sperm
556 downregulate DSB induction. Taken together, our study supports a model in which signals due
557 to sperm depletion and reproductive aging operate in parallel to influence meiotic DSB induction
558 and repair (Figure 7).

559 **Sperm depletion and DSB induction**

560 Our data indicate that aged unmated germlines exhibit dramatically reduced RAD-51 foci
561 in early pachytene (Figure 7). Previous work has similarly reported that unmated
562 hermaphrodites induce fewer DSBs with age (Achache *et al.* 2021; Raices *et al.* 2021). We find,
563 however, that mating is sufficient to rescue RAD-51 foci accumulation at early pachytene in
564 aged germlines. This effect in mated hermaphrodites may be due to cues from sperm-specific
565 signals, seminal fluid components, or male pheromones, all of which impact hermaphrodite
566 physiology (Shi and Murphy 2014; Aprison *et al.* 2022). While our study cannot distinguish
567 between these male- and mating-dependent effects, it is notable that aged feminized *fog-2*
568 germlines, which have never been exposed to sperm or males, do not exhibit reduced RAD-51
569 marked DSBs during aging. Thus, we propose that DSB induction in aged germlines is primarily
570 repressed by signals caused specifically from sperm depletion rather than reproductive aging,
571 mating-induced signaling, or exposure to males. We further found that *spo-11(me44)* mutants
572 do not exhibit increased DSBs with age, suggesting that the DSBs observed in aged gonads
573 come from the endogenous meiotic machinery. This result contrasts with previous work done
574 using *spo-11(ok79)* mutants, which incur SPO-11 independent DSBs with age (Raices *et al.*
575 2021). Thus, our data raises the possibility that the specific nature of *spo-11* mutation or
576 background strain-specific effects influence the occurrence of exogenous DSBs in aged
577 germlines.

578 Why might sperm depleted hermaphrodites downregulate germline DSB induction?
579 Recent evidence has unveiled a potential transition in hermaphrodite gonad function following

580 sperm depletion (Kern *et al.* 2021). After all sperm have been utilized from the spermatheca,
581 hermaphrodites continue to lay unfertilized oocytes and secrete a nutrient-rich yolk in what has
582 been suggested to be a form of 'primitive lactation' (Kern *et al.* 2021). Thus, the reduction in
583 DSBs induced in germ cells following sperm depletion may be a product of the hermaphrodite
584 germline functionally changing from a reproductive organ to a system which produces food for
585 offspring. Reduced DSB formation, then, may be indicative of the metabolic resources of the
586 hermaphrodite being reallocated in favor of providing nutritional supplement for progeny.
587 Multiple mutants in *C. elegans* have been reported to exhibit age-dependent decline in
588 meiotic DSB induction (Tang *et al.* 2010; Rosu *et al.* 2013). Our research raises the possibility
589 that these proteins may mediate or respond to signals from sperm. Also, both reproductive
590 aging and *C. elegans* yolk secretion are regulated by insulin/insulin-like growth factor signaling
591 (Luo *et al.* 2010; Kern *et al.* 2021). How reproductive aging and sperm depletion signals are
592 integrated through this pathway to enact distinct phenotypes that impact germline function
593 remains unknown but opens an avenue for future investigation. In summary, we have
594 illuminated a regulatory mechanism specifically associated with sperm depletion which
595 downregulates DSB induction in the *C. elegans* germline.
596 **DSB repair and *C. elegans* reproductive aging**
597 Aged *C. elegans* germlines exhibit multiple DNA repair defects, including delays in
598 recombination protein loading and increased engagement of error-prone repair mechanisms
599 (Raices *et al.* 2021). Both RAD-51 loading and error prone pathway engagement are regulated
600 by DSB end resection (Gartner and Engebrecht 2022), suggesting that differences in DSB
601 repair during aging may be derived from defects at this DNA processing step. We demonstrate
602 that the E2 ligase variant UEV-2 is required for 'youthful' patterns of RAD-51 foci resolution
603 during mid pachytene, indicating that a loss of UEV-2 or an age-related change in its function
604 may underly the DNA repair defects in aged germlines. However, overexpression of UEV-2 is
605 not sufficient to rescue persistent RAD-51 foci at mid pachytene in aged germlines and instead

606 introduces DSB repair defects in young germlines. These results suggest that the specific
607 levels of *uev-2* expression or the co-expression of other proteins may be important for the
608 function of UEV-2 in DNA repair processes.

609 While the specific molecular functions of UEV-2 remain unknown, previous yeast two-
610 hybrid assays have evidenced that UEV-2 may interact with BRC-1, the *C. elegans* BRCA1
611 homolog (Gudgen *et al.* 2004). BRCA1 is an E3 ubiquitin ligase thought to regulate many DNA
612 repair steps, including DSB resection (Cruz-García *et al.* 2014). Recent studies have
613 demonstrated that BRC-1 is vital for preventing error prone repair in the *C. elegans* germline (Li
614 *et al.* 2020; Kamp *et al.* 2020). Given these results, we propose that UEV-2 may modulate BRC-
615 1 activity in the germline to regulate resection of DSBs and promote efficient recombination.
616 Under this model, overexpression of *uev-2* or loss of its function may cause hyper- or hypo-DSB
617 resection respectively, and thus have a deleterious impact on the efficiency of recombination.
618 Taken together, our work demonstrates that UEV-2 is involved in regulating efficient and
619 'youthful' meiotic DSB repair, thereby opening avenues to future work uncovering the specific
620 roles this protein plays in meiosis.
621

622 **Acknowledgements**

623 We thank the CGC (funded by National Institutes of Health (NIH) P40 OD010440) for strains.
624 We thank C. Cahoon, A. Naftaly, and N. Kurhanewicz for thoughtful comments on this
625 manuscript. This work was supported by the National Institutes of Health T32GM007413 and
626 Advancing Science in America (ARCS) Foundation Award to E.T., and National Institutes of
627 Health R00HD076165 and R35GM128890 to D.E.L. D.E.L. is also a recipient of a March of
628 Dimes Basil O'Connor Starter Scholar award and Searle Scholar Award.
629

630 **Competing Interests**

631 The authors declare no competing interests.

632

633 **Figures**

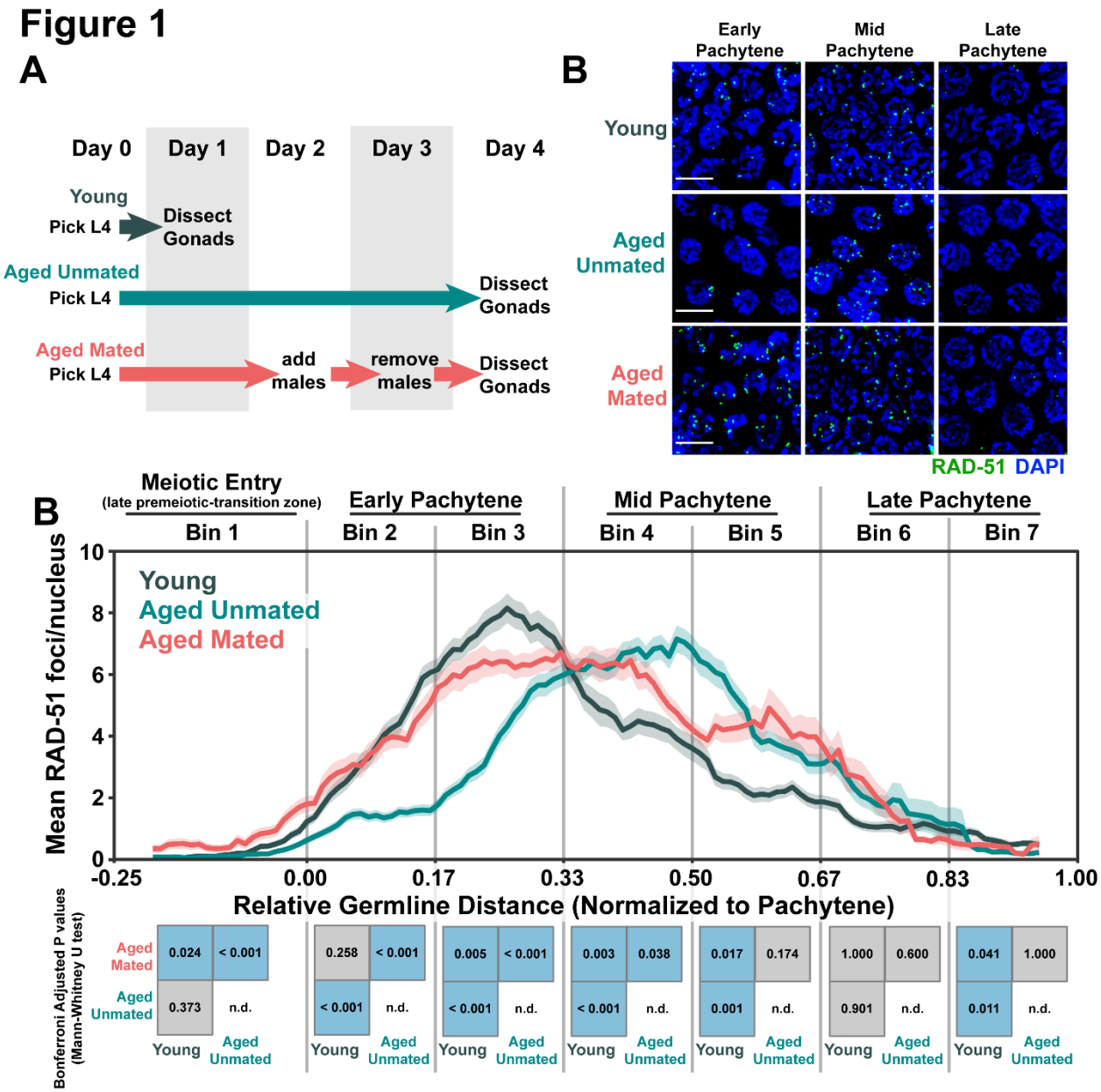

634

635 **Figure 1. DNA double strand break levels are altered during *C. elegans* germline aging.** A)

636 Schemes used to isolate young (1 day post-L4) and aged (4 days post L4) worms for

637 experiments. Days count ~18-24 hour periods after hermaphrodites were isolated as L4 larvae

638 and are separated by alternating grey shaded boxes. B) Representative images of RAD-51 foci

639 meiotic nuclei in young and aged germlines. Scale bars represent 5μm. C) RAD-51 foci per

640 nucleus in oocytes. Line plots represent the mean RAD-51 foci per nucleus along the length of
641 the germline in a sliding window encompassing 0.1 units of normalized germline distance with a
642 step size of 0.01 germline distance units. Mean RAD-51 foci were calculated from nuclei
643 analyzed in n=9 total germlines derived from ≥3 experimental replicates within each age group.
644 Shaded areas around each line represent ± SEM. Total nuclei analyzed (Bins 1/2/3/4/5/6/7)
645 Young: 185/117/146/107/117/97/83; Aged Mated: 234/205/192/173/154/177/96; Aged Unmated:
646 268/147/161/175/191/152/110. Germlines distances were normalized to the start (0) and end (1)
647 of pachytene based on DAPI morphology (see Methods). For analysis, the germline was divided
648 into 7 bins encompassing the transition zone (Bin 1), early pachytene (Bins 2-3), mid pachytene
649 (Bins 4-5), and late pachytene (Bins 6-7). The germline positions at which each bin start and
650 end are marked on the X axis as vertical grey lines. Heat maps below each bin display the p
651 values of pairwise comparisons of RAD-51 foci per nucleus counts within that bin. P values
652 were calculated using Mann-Whitney U tests with Bonferroni correction for multiple
653 comparisons. Blue tiles indicate significant differences (adjusted p value <0.05) and grey tiles
654 indicate nonsignificant effects (adjusted p value >0.05).

655

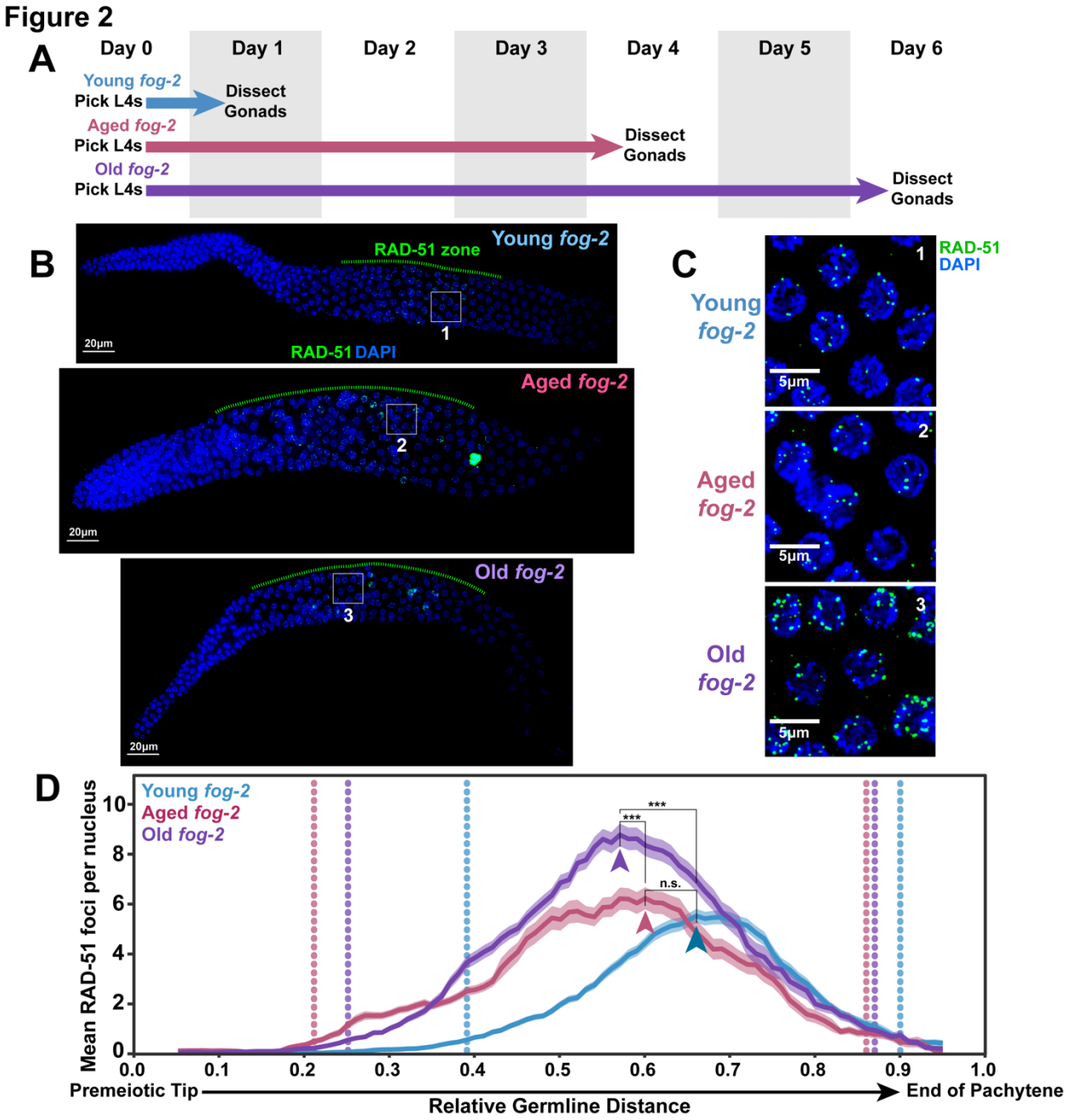

Figure 2. DNA double strand break levels increase with age in *fog-2* feminized germlines. A) Schemes used to isolate young (1 day post-L4), aged (4 days post L4), and old (6 days post L4) *fog-2(q71)* worms for experiments. Days count ~18-24 hour periods after hermaphrodites were isolated as L4 larvae and are separated by alternating grey shaded boxes. B) Representative whole germline images of young, aged, and old *fog-2* germlines. The RAD-51

662 zone, defined as the region of the germline in which the majority of nuclei have one or more
663 RAD-51 foci, is indicated with a green dashed line. All germlines are oriented with the distal
664 mitotic tip on the left and the end of pachytene on the right. Scale bars represent 20μm. Grey
665 numbered boxes indicate the positions of the images presented in panel C. C) Representative
666 images of the peak levels of RAD-51 foci observed in meiotic nuclei of young, aged, and old
667 *fog-2* germlines. Scale bars represent 5μm. Each panel is numbered to indicate the position in
668 the germlines displayed in panel B that each inset was taken from. D) RAD-51 foci per nucleus
669 in *fog-2(q71)* oocytes. Line plots represents the mean RAD-51 foci per nucleus along the length
670 of the germline in a sliding window encompassing 0.1 units of normalized germline distance with
671 a step size of 0.01 germline distance units. Mean RAD-51 foci were calculated from nuclei
672 analyzed in n=9 total germlines derived from ≥3 experimental replicates within each age group.
673 Shaded areas around each line represent ± SEM. Average nuclei quantified in each bin ±
674 standard deviation: Young *fog-2* 173±21.3, Aged *fog-2* 143±32.0, Old *fog-2* 148.5±29.6.
675 Germline distance was normalized to the premeiotic tip (0) and end of pachytene (1) based on
676 DAPI morphology (see Methods). Arrowheads indicate the "peak RAD-51" windows, defined as
677 the windows along the length of the germline of each age group with the highest RAD-51 foci
678 per nucleus. P values were calculated by Mann-Whitney U test comparisons of RAD-51 counts
679 within these peak windows with Bonferroni correction for multiple comparisons (n.s. = $p>0.05$,
680 *** = $p<0.001$). Vertical dotted lines indicate the distal and proximal bounds of the RAD-51 zone
681 for each age group, defined as windows in which the median RAD-51 foci per nucleus count
682 was ≥1.
683

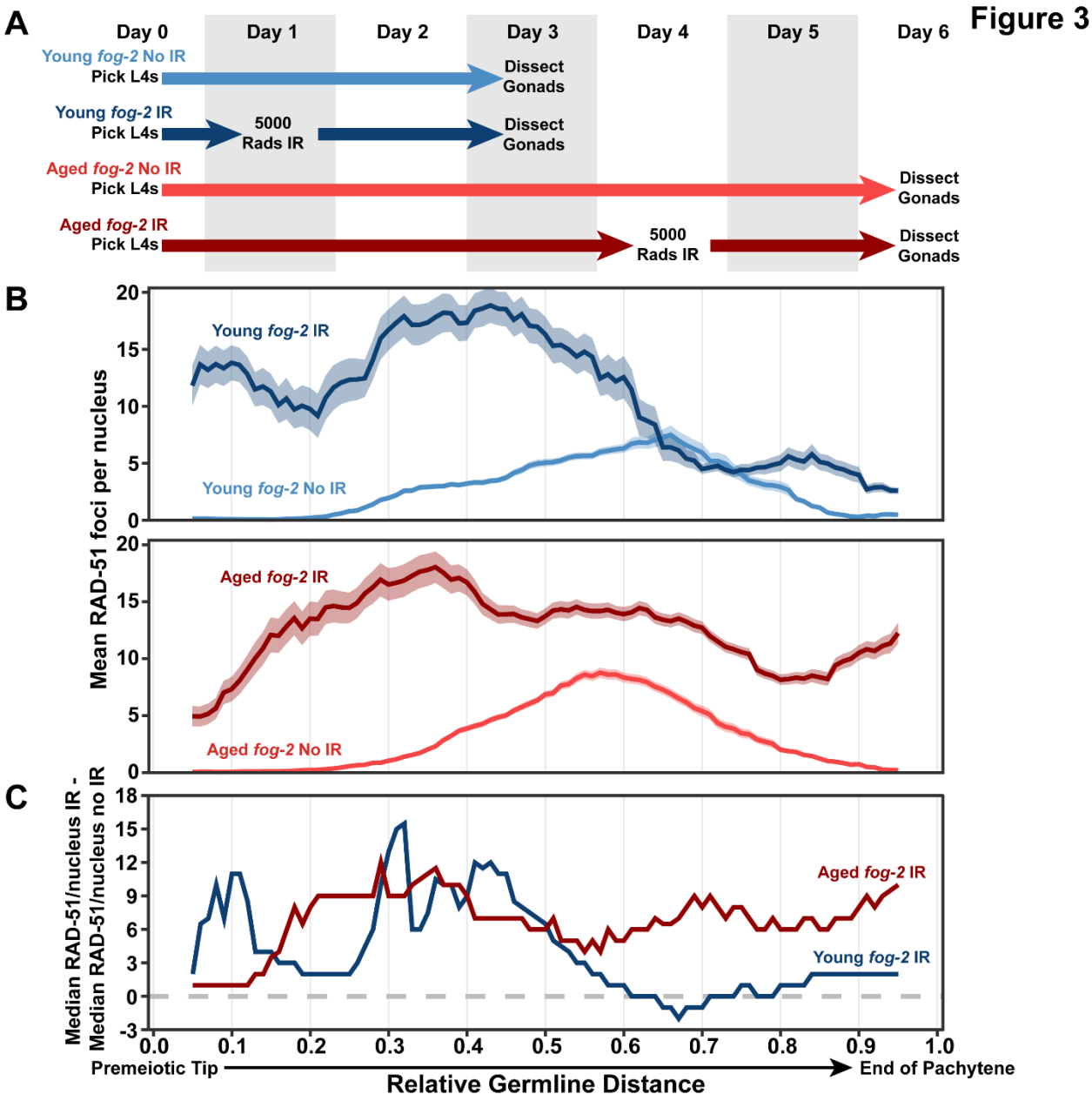

684

685 **Figure 3. DNA double strand break repair is disrupted in aged *fog-2* feminized germlines.**

686 A) Schemes used to isolate young and aged *fog-2(q71)* worms for experiments. Days count

687 ~18-24 hour periods after hermaphrodites were isolated as L4 larvae and are separated by

688 alternating grey shaded boxes. Irradiated (IR) germlines were exposed to ionizing radiation at

689 the first or fourth day of adulthood and were allowed to recover for two days before analysis

690 (see Methods). Unirradiated germlines (No IR) were never exposed to radiation. B) RAD-51 foci

691 per nucleus in irradiated (IR) and unirradiated (no IR) oocytes. Line plots represents the mean
692 RAD-51 foci per nucleus along the length of the germline in a sliding window encompassing 0.1
693 units of normalized germline distance with a step size of 0.01 germline distance units. Plots in
694 panel B share an X axis with the plot in panel C. Mean RAD-51 foci were calculated from nuclei
695 analyzed in n=9 total germlines derived from ≥3 experimental replicates within each age group.
696 Shaded areas around each line represent ± SEM. Average nuclei quantified in each bin ±
697 standard deviation: Young *fog-2* No IR 141.6±26.6, Young *fog-2* IR 134.4±27.9, Old *fog-2* No IR
698 148.5±29.6, Old *fog-2* IR 142.4±30. Germline distance was normalized to the premeiotic tip (0)
699 and end of pachytene (1) based on DAPI morphology (see Methods). Representative images of
700 young and aged IR and No IR germlines are displayed in Supplemental Figure 5. C) Median
701 RAD-51 foci per nucleus in irradiated germlines above median levels in unirradiated germlines
702 of the same age (calculated as median RAD-51 foci in IR gonads – median RAD-51 foci in non-
703 IR gonads within each window along the length of the germline).

704

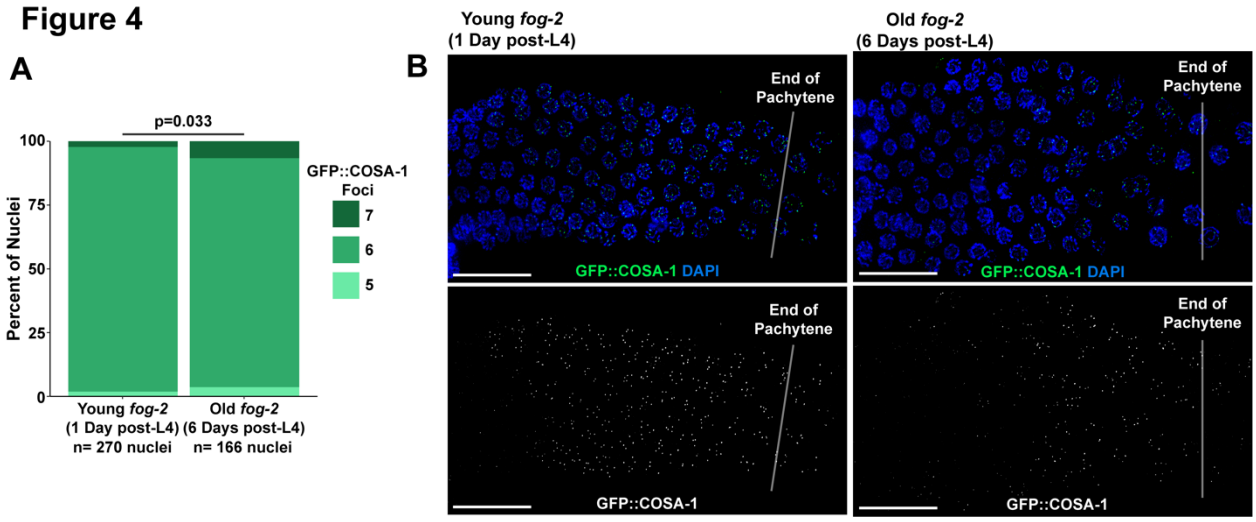

705

706 **Figure 4. Crossover designation is altered in aged *fog-2* germlines.** A) Stacked bar plot of
707 the percent of nuclei in young (1 day post L4) and old (6 days post L4) *fog-2* mutants with the
708 given number of GFP::COSA-1 foci. The p value displayed was calculated by Chi Square test. N
709 values indicate the number of nuclei scored. B) Representative images of GFP::COSA-1
710 localization in young and old *fog-2* mutant germlines. Scale bars represent 20μm. Germlines are
711 oriented with the proximal end on the left and distal end on the right. Vertical low opacity white
712 lines designate the end of pachytene.

713

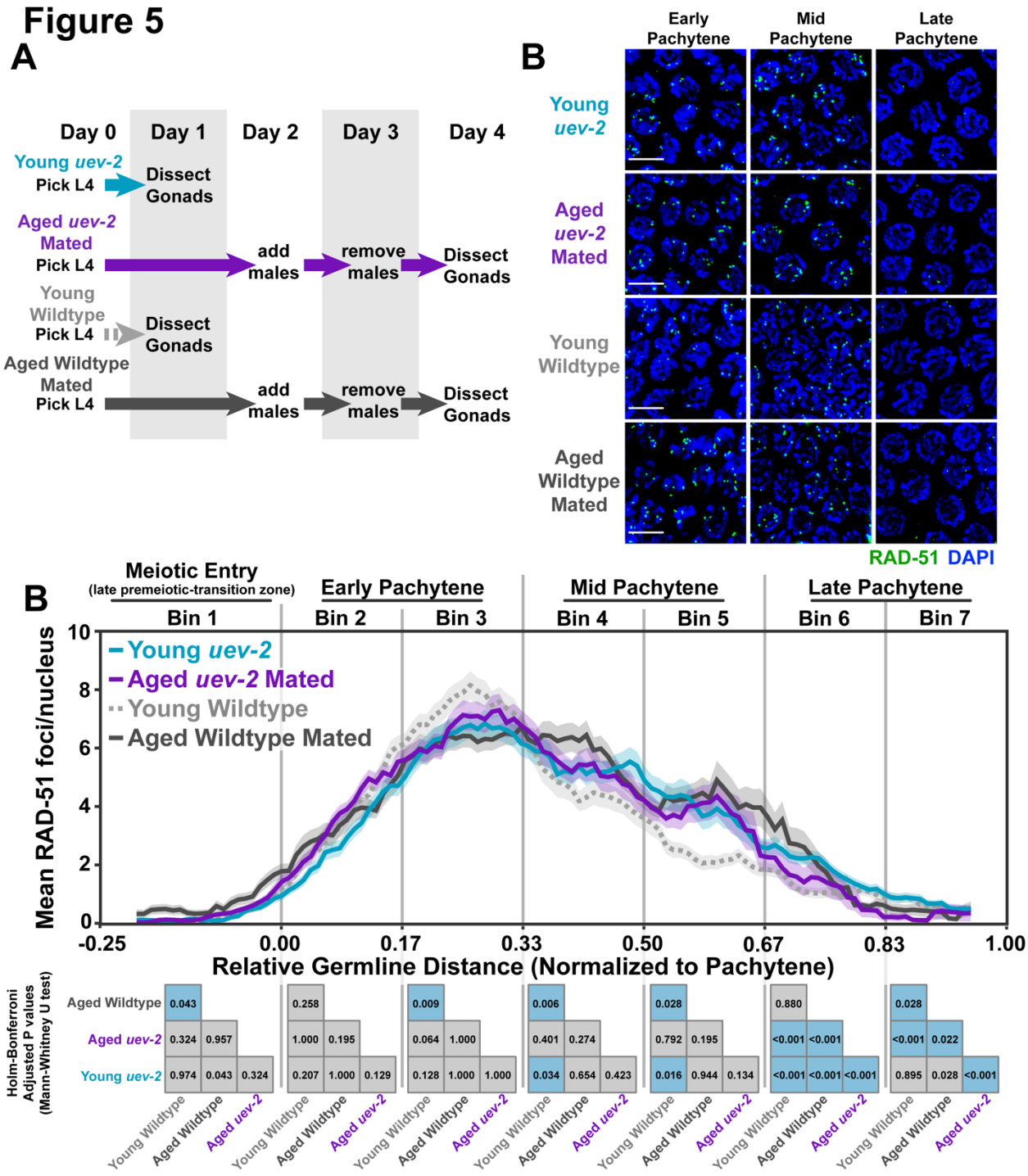

Figure 5. UEV-2 is required for 'youthful' DNA repair. A) Schemes used to isolate young (1 day post-L4) and aged (4 days post L4) *uev-2* mutant worms for experiments. Days count ~18-24 hour periods after hermaphrodites were isolated as L4 larvae and are separated by alternating grey shaded boxes. B) Representative images of RAD-51 foci in meiotic nuclei of

young *uev-2*, aged mated *uev-2*, young wildtype, and aged mated wildtype germlines. Scale bars represent 5μm. C) RAD-51 foci per nucleus in oocytes. Line plots represent the mean RAD-51 foci per nucleus along the length of the germline in a sliding window encompassing 0.1 units of normalized germline distance with a step size of 0.01 germline distance units. Mean RAD-51 foci were calculated from nuclei analyzed in n=9 total germlines derived from ≥3 experimental replicates within each age and genotype group. Shaded areas around each line represent ± SEM. Total nuclei analyzed (Bins 1/2/3/4/5/6/7) Young Wildtype: 185/117/146/107/117/97/83; Aged Wildtype Mated: 234/205/192/173/154/177/96; Young *uev-2*: 186/135/134/113/112/132/95; Aged *uev-2* Mated: 129/161/155/158/167/142/120. Germlines distances were normalized to the start (0) and end (1) of pachytene based on DAPI morphology (see Methods). For analysis, the germline was divided into 7 bins encompassing the transition zone (Bin 1), early pachytene (Bins 2-3), mid pachytene (Bins 4-5), and late pachytene (Bins 6-7). The germline positions at which each bin start and end are marked on the X axis as vertical grey lines. Heat maps below each bin display the p values of pairwise comparisons of RAD-51 foci per nucleus counts within that bin. P values were calculated using Mann-Whitney U tests with Holm-Bonferroni correction for multiple comparisons. Blue tiles indicate significant differences (adjusted p value <0.05) and grey tiles indicate nonsignificant effects (adjusted p value >0.05).

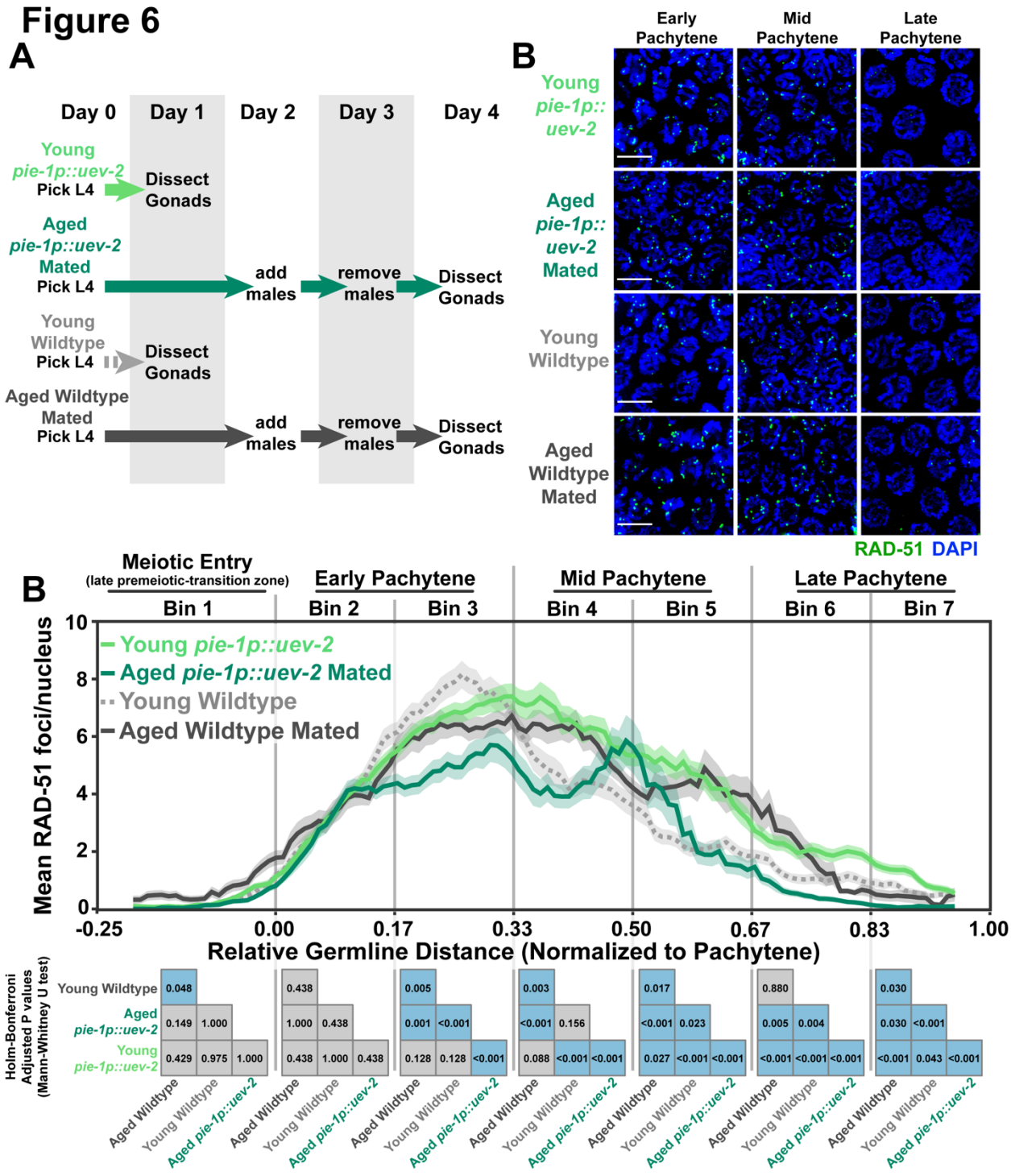

Figure 6. Germline *uev-2* overexpression differentially impacts DSB levels in young and aged germlines. A) Schemes used to isolate young (1 day post-L4) and aged (4 days post L4) worms for experiments. Days count ~18-24 hour periods after hermaphrodites were isolated as

742 L4 larvae and are separated by alternating grey shaded boxes. B) Representative images of
743 RAD-51 foci in meiotic nuclei of young *pie-1p::uev-2*, aged *pie-1::uev-2*, and young wildtype
744 germlines. Scale bars represent 5μm. C) RAD-51 foci per nucleus in oocytes. Line plots
745 represent the mean RAD-51 foci per nucleus along the length of the germline in a sliding
746 window encompassing 0.1 units of normalized germline distance with a step size of 0.01
747 germline distance units. Mean RAD-51 foci were calculated from nuclei analyzed in n=9 total
748 germlines derived from ≥3 experimental replicates within each age group. Shaded areas around
749 each line represent ± SEM. Total nuclei analyzed (Bins 1/2/3/4/5/6/7) Young Wildtype:
750 185/117/146/107/117/97/83; Aged Wildtype Mated: 234/205/192/173/154/177/96; Young *pie-*
751 *1p::uev-2*: 182/192/162/125/116/97; Aged *pie-1p::uev-2* Mated: 140/149/136/127/126/95/102.
752 Germlines distances were normalized to the start (0) and end (1) of pachytene based on DAPI
753 morphology (see Methods). For analysis, the germline was divided into 7 bins encompassing
754 the transition zone (Bin 1), early pachytene (Bins 2-3), mid pachytene (Bins 4-5), and late
755 pachytene (Bins 6-7). The germline positions at which each bin start and end are marked on the
756 X axis as vertical grey lines. Heat maps below each bin display the p values of pairwise
757 comparisons of RAD-51 foci per nucleus counts within that bin. P values were calculated using
758 Mann-Whitney U tests with Holm-Bonferroni correction for multiple comparisons. Blue tiles
759 indicate significant differences (adjusted p value <0.05) and grey tiles indicate nonsignificant
760 effects (adjusted p value >0.05).

761

Figure 7

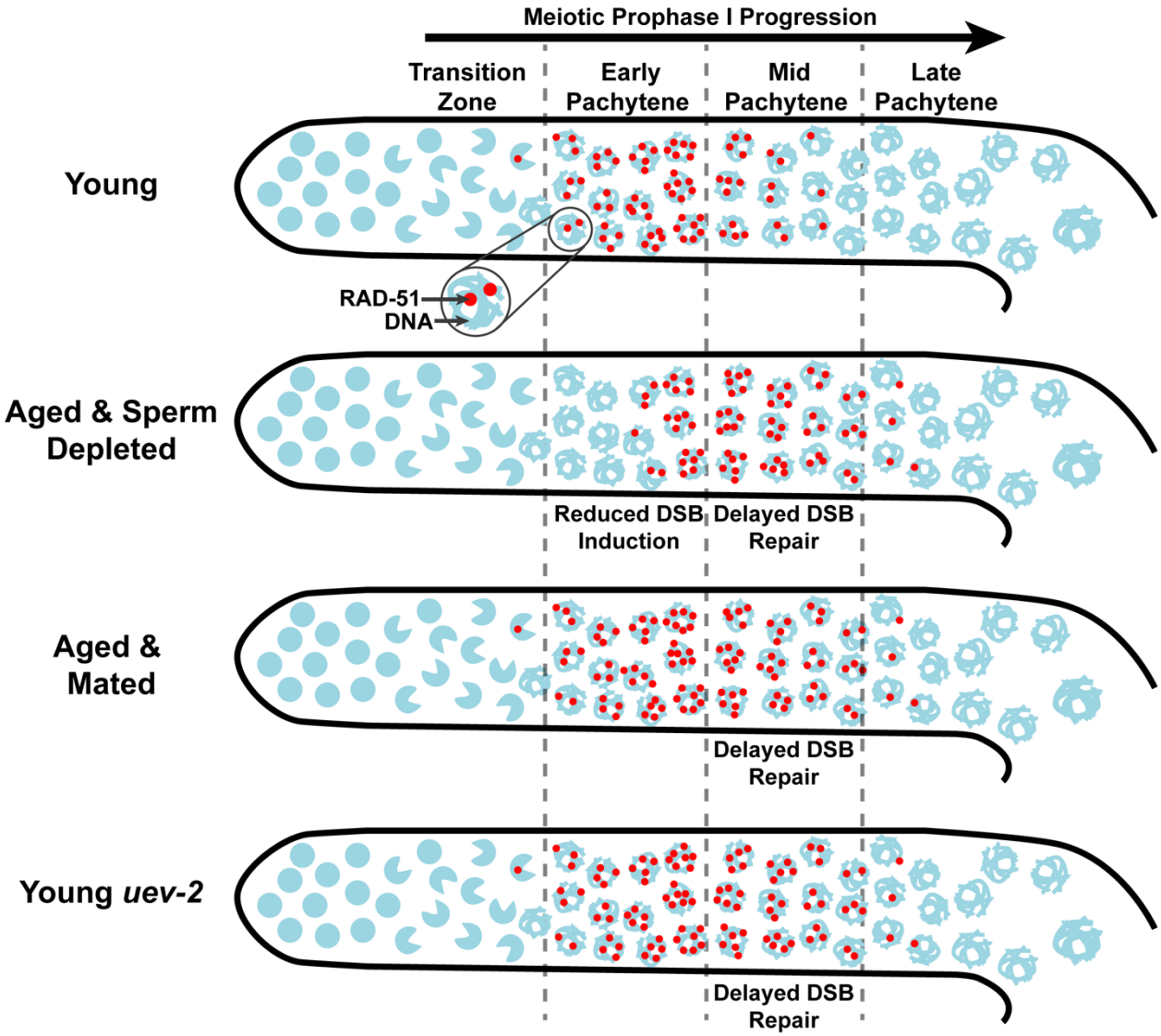

762

763 **Figure 7. Model of aging and sperm effects on DSB levels during germline aging.**

764 **References**

765 Achache H., R. Falk, N. Lerner, T. Beatus, and Y. B. Tzur, 2021 Oocyte aging is controlled by
766 mitogen-activated protein kinase signaling. Aging Cell 20.

767 Albert Hubbard E. J., and D. Greenstein, 2000 The Caenorhabditis elegans gonad: A test tube
768 for cell and developmental biology. Dev. Dyn. 218: 2–22.

769 Andux S., and R. E. Ellis, 2008 Apoptosis maintains oocyte quality in aging Caenorhabditis
770 elegans females. PLoS Genet. 4.

771 Angeles-Albores D., D. H. W. Leighton, T. Tsou, T. H. Khaw, I. Antoshechkin, *et al.*, 2017 The
772 Caenorhabditis elegans female-like state: Decoupling the transcriptomic effects of aging
773 and sperm status. G3 Genes, Genomes, Genet. 7: 2969–2977.

774 Aprison E. Z., S. Dzitoyeva, and I. Ruvinsky, 2022 Serotonin coordinates reproductive functions
775 in Caenorhabditis. BioRXiv.

776 Broekmans F. J., E. A. H. Knauff, E. R. te Velde, N. S. Macklon, and B. C. Fauser, 2007 Female
777 reproductive ageing: current knowledge and future trends. Trends Endocrinol. Metab. 18:
778 58–65.

779 Cahoon C. K., J. M. Helm, and D. E. Libuda, 2019 Synaptonemal Complex Central Region
780 Proteins Promote Localization of Pro-crossover Factors to Recombination Events During
781 Caenorhabditis elegans Meiosis. Genetics 213: 395–409.

782 Chatzidaki E. E., S. Powell, B. J. H. Dequeker, J. Gassler, M. C. C. Silva, *et al.*, 2021 Ovulation
783 suppression protects against chromosomal abnormalities in mouse eggs at advanced
784 maternal age. Curr. Biol. 31: 4038-4051.e7.

785 Cinquin A., M. Chiang, A. Paz, S. Hallman, O. Yuan, *et al.*, 2016 Intermittent Stem Cell Cycling
786 Balances Self-Renewal and Senescence of the C. elegans Germ Line. PLoS Genet. 12.

787 Colaiácovo M. P., A. J. MacQueen, E. Martinez-Perez, K. McDonald, A. Adamo, *et al.*, 2003
788 Synaptonemal complex assembly in C. elegans is dispensable for loading strand-exchange
789 proteins but critical for proper completion of recombination. Dev. Cell 5: 463–474.

790 Cruz-García A., A. López-Saavedra, and P. Huertas, 2014 BRCA1 accelerates CtIP-ediated
791 DNA-end resection. Cell Rep. 9: 451–459.

792 Dernburg A. F., K. McDonald, G. Moulder, R. Barstead, and M. Dresser, 1998 Meiotic
793 Recombination in C. elegans Initiates by a Conserved Mechanism and Is Dispensable for
794 Homologous Chromosome Synapsis. Cell 94: 387–389.

795 Doniach T., and J. Hodgkin, 1984 A Sex-Determining Gene, fem-1, Required for Both Male and
796 Hermaphrodite Development in Caenorhabditis elegans. Dev. Biol. 106: 223–235.

797 Gartner A., and J. A. Engebrecht, 2022 DNA repair, recombination, and damage signaling.
798 Genetics 220.

799 Gudgen M., A. Chandrasekaran, T. Frazier, and L. Boyd, 2004 Interactions within the ubiquitin
800 pathway of Caenorhabditis elegans. Biochem. Biophys. Res. Commun. 325: 479–486.

801 Kamp J. A., R. van Schendel, I. W. Dilweg, and M. Tijsterman, 2020 BRCA1-associated
802 structural variations are a consequence of polymerase theta-mediated end-joining. Nat.
803 Commun. 11: 1–10.

804 Keeney S., C. N. Giroux, and N. Kleckner, 1997 Meiosis-Specific DNA Double-Strand Breaks
805 Are Catalyzed by Spo11, a Member of a Widely Conserved Protein Family. Cell 88: 375–
806 384.

807 Kern C. C., S. J. Townsend, A. Salzmann, N. B. Rendell, G. W. Taylor, *et al.*, 2021 C. elegans
808 feed yolk to their young in a form of primitive lactation. Nat. Commun. 12.

809 L'Hernault S. W., 2006 Spermatogenesis. WormBook 1–14.

810 Li Q., S. Hariri, and J. Engebrecht, 2020 Meiotic double-strand break processing and crossover
811 patterning are regulated in a sex-specific manner by BRCA1-BARD1 in C. elegans.
812 Genetics 216: 359–379.

813 Libuda D. E., S. Uzawa, B. J. Meyer, and A. M. Villeneuve, 2013 Meiotic chromosome
814 structures constrain and respond to designation of crossover sites. Nature 502: 703–706.

815 Luo S., W. M. Shaw, J. Ashraf, and C. T. Murphy, 2009 TGF-ß Sma/Mab signaling mutations
816 uncouple reproductive aging from somatic aging. PLoS Genet. 5.

817 Luo S., G. A. Kleemann, J. M. Ashraf, W. M. Shaw, and C. T. Murphy, 2010 TGF-β and Insulin
818 Signaling Regulate Reproductive Aging via Oocyte and Germline Quality Maintenance. Cell
819 143: 299–312.

820 Mack H. I. D., T. Heimbucher, and C. T. Murphy, 2018 The nematode Caenorhabditis elegans
821 as a model for aging research. Drug Discov. Today Dis. Model. 27: 3–13.

822 Maures T. J., L. N. Booth, B. A. Benayoun, Y. Izrayelit, F. C. Schroeder, *et al.*, 2014 Males
823 shorten the life span of C. elegans hermaphrodites via secreted compounds. Science (80-.
824). 343: 541–544.

825 Mccarter J., B. Bartlett, T. Dang, and T. Schedl, 1999 On the Control of Oocyte Meiotic
826 Maturation and Ovulation in Caenorhabditis elegans. Dev. Biol. 205: 111–128.

827 Moghadam A. R. E., M. T. Moghadam, M. Hemadi, and G. Saki, 2022 Oocyte quality and aging.
828 J. Bras. Reprod. Assist. 26: 105–122.

829 Pickett C. L., and K. Kornfeld, 2013 Age-related degeneration of the egg-laying system
830 promotes matricidal hatching in Caenorhabditis elegans. Aging Cell 12: 544–553.

831 Preibisch S., S. Saalfeld, and P. Tomancak, 2009 Globally optimal stitching of tiled 3D
832 microscopic image acquisitions. Bioinforma. Appl. 25: 1463–1465.

833 Raices M., R. Bowman, S. Smolikove, and J. L. Yanowitz, 2021 Aging Negatively Impacts DNA
834 Repair and Bivalent Formation in the C. elegans Germ Line. Front. Cell Dev. Biol. 9.

835 Rosu S., K. A. Zawadzki, E. L. Stamper, D. E. Libuda, and A. L. Reese, 2013 The C. elegans
836 DSB-2 Protein Reveals a Regulatory Network that Controls Competence for Meiotic DSB
837 Formation and Promotes Crossover Assurance. PLoS Genet 9: 1–23.

838 Ruth K. S., F. R. Day, J. Hussain, A. Martínez-Marchal, C. E. Aiken, *et al.*, 2021 Genetic
839 insights into biological mechanisms governing human ovarian ageing. Nature 596: 393–
840 397.

841 Sancho E., M. R. Vila, L. Sanchez-Pulido, J. J. Lozano, R. Paciucci, *et al.*, 1998 Role of UEV-1,
842 an Inactive Variant of the E2 Ubiquitin-Conjugating Enzymes, in In Vitro Differentiation and
843 Cell Cycle Behavior of HT-29-M6 Intestinal Mucosecretory Cells. Mol. Cell. Biol. 18: 576–
844 589.

845 Schedl T., and J. Kimble, 1988 fog-2, a Germ-Line-Specific Sex Determination Gene Required
846 for Hermaphrodite Spermatogenesis in Caenorhabditis elegans. Genetics 119: 46–61.

847 Shi C., and C. T. Murphy, 2014 Mating Induces Shrinking and Death in *Caenorhabditis* Mothers.
848 Science (80-.). 343: 536–540.

849 Shim E. Y., A. K. Walker, and T. Keith Blackwell, 2002 Broad requirement for the mediator
850 subunit RGR-1 for transcription in the Caenorhabditis elegans embryo. J. Biol. Chem. 277:
851 30413–30416.

852 Silva-García C. G., A. Lanjuin, C. Heintz, S. Dutta, N. M. Clark, *et al.*, 2019 Single-copy knock-in
853 loci for defined gene expression in caenorhabditis elegans. G3 Genes, Genomes, Genet.
854 9: 2195–2198.

855 Tang L., T. Machacek, Y. M. Mamnun, A. Penkner, J. Gloggnitzer, *et al.*, 2010 Mutations in
856 Caenorhabditis elegans him-19 Show Meiotic Defects That Worsen with Age. Mol. Biol.

857 Cell 21: 885–896.

858 Thompson O., M. Edgley, P. Strasbourger, S. Flibotte, B. Ewing, *et al.*, 2013 The million
859 mutation project: A new approach to genetics in Caenorhabditis elegans. Genome Res. 23:
860 1749–1762.

861 Toraason E., V. L. Adler, N. A. Kurhanewicz, A. DiNardo, A. M. Saunders, *et al.*, 2021
862 Automated and customizable quantitative image analysis of whole Caenorhabditis elegans
863 germlines. Genetics 217.

864 Vandemark A. P., R. M. Hofmann, C. Tsui, C. M. Pickart, and C. Wolberger, 2001 Molecular
865 Insights into Polyubiquitin Chain Assembly: Crystal Structure of the Mms2/Ubc13
866 Heterodimer. Cell 105: 711–720.

867 Wasserzug-Pash P., R. Rothman, E. Reich, L. Zecharyahu, O. Schonberger, *et al.*, 2022 Loss
868 of heterochromatin and retrotransposon silencing as determinants in oocyte aging. Aging
869 Cell 21.

870 Wickham H., M. Averick, J. Bryan, W. Chang, L. McGowan, *et al.*, 2019 Welcome to the
871 Tidyverse. J. Open Source Softw. 4: 1686.

872 Wijk S. J. L., and H. T. M. Timmers, 2010 The family of ubiquitin-conjugating enzymes (E2s):
873 deciding between life and death of proteins. FASEB J. 24: 981–993.

874 Yokoo R., K. A. Zawadzki, K. Nabeshima, M. Drake, S. Arur, *et al.*, 2012 COSA-1 Reveals
875 Robust Homeostasis and Separable Licensing and Reinforcement Steps Governing
876 Meiotic Crossovers. Cell 149: 75–87.

877